Macromolecules

pubs.acs.org/Macromolecules

Article

Raman Fingerprints of π-Electron Delocalization in Polythiophene-Based Insulated Molecular Wires

Sara Mosca, Alberto Milani, Chiara Castiglioni,* Víctor Hernández Jolín, Cristóbal Meseguer, Juan T. López Navarrete, Chunhui Zhao, Kazunori Sugiyasu, and M. Carmen Ruiz Delgado*

Cite This: *Macromolecules* 2022, 55, 3458–3468

Read Online

ACCESS | Metrics & More | Article Recommendations | Supporting Information

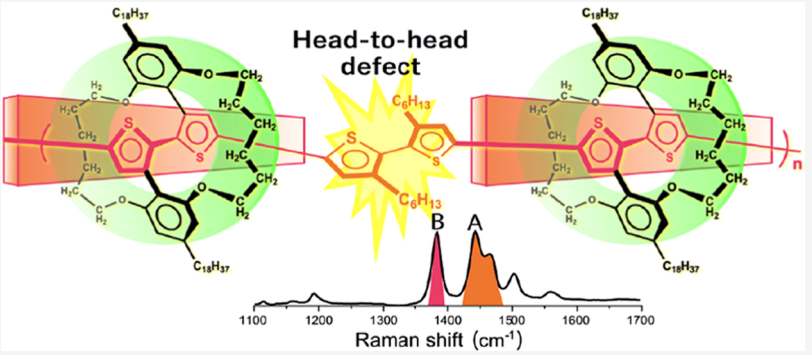

ABSTRACT: Insulated polythiophenes with a polyrotaxane-like 3D architecture have shown excellent intrawire hole mobility, allowing their use in interesting optoelectronic applications. This is due to the isolation of the π-conjugated backbones that warrants for stabilization of the quasi-planar conformation of the polythiophene core and prevents electronic communication between adjacent chains. Thus, polythiophene-based insulated molecular wires (IMWs) constitute ideal test-beds to evaluate the structural changes within the conjugated polymer chain, such as intrachain conformation and π-electron delocalization. Here, we investigate the structure and spectroscopic response of fully and partially insulated polythiophene-based IMWs. An experimental investigation of Raman spectra supported by density functional theory (DFT) calculations allows us to give a detailed interpretation of intramolecular interactions, highlighting differences in π-electron conjugation revealed by the presence of an intensity transfer between the two main Raman modes associated with the C═C/C−C stretching vibrations. This study proves the sensitivity of Raman spectroscopy as a technique to monitor structural changes in self-encapsulated conjugated polymers.

INTRODUCTION

Conjugated polymers (CPs) and oligomers have become largely used in organic devices[1,2] as plastic electronics and photovoltaic materials[3] due to their interesting properties. They can be used as active materials in light-emitting diodes[4] or as labeling agents in biological applications[5] due to their good light-absorbing and light-emitting properties and their great environmental sensitivity. Alternatively, CPs could also be used as organic field-effect transistors (OFETs) thanks to their charge transport properties.[6] In all of these applications, the structure of CP chains and their interaction can have significant effects on their properties that reflect on the device's performance. For example, structural defects along the polymer backbone or conformational disorder could limit π-electron delocalization, thus also affecting its conducting properties.[7,8] Moreover, the material morphology and the related interchain interactions can remarkably affect the charge transport efficiency and electrical conductivity.[8−10] On these grounds, the understanding of the molecular structure is crucial for in-depth knowledge of that class of material and allows us to clarify the relation among the supramolecular architecture, chain conformation, π-electron delocalization, and the optical/electronic properties of conjugated materials. Within this context, Raman spectroscopy is a powerful tool for characterizing the structural order in polyconjugated materials in conjunction with long-range interactions or confinement of π-electrons.[9] Indeed, the most significant Raman transitions in conjugated molecules are associated with collective out-of-phase (C═C/C−C) stretching vibrations and are often referred to as Я modes, according to the effective conjugation coordinate (ECC) theory by Zerbi et al.[9,11,12] The Я modes are oscillations of the bond length alternation (BLA) along the

Received: December 2, 2021
Revised: March 10, 2022
Published: April 22, 2022

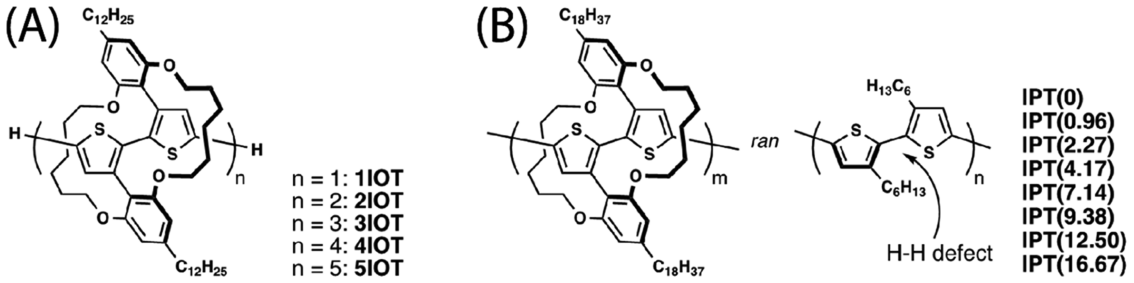

Figure 1. Chemical structure of insulated oligothiophenes (**nIOT**) and polythiophene (**IPT(N)**): (A) defect-free oligomers **nIOT** with bithiophene-based repetition units n = 1−5, (B) copolymers **IPT(N)** with a determined percentage (N%) of head-to-head defect units consisting of 3,3′-dihexyl-2,2′-bithiophene. The defect percentage indicated in parentheses is defined as $N = [n/(2m + 2n)] \times 100$.

Scheme 1. Synthetic Route to Insulated Polythiophene with Head-to-Head Defects: IPT(N)[a]

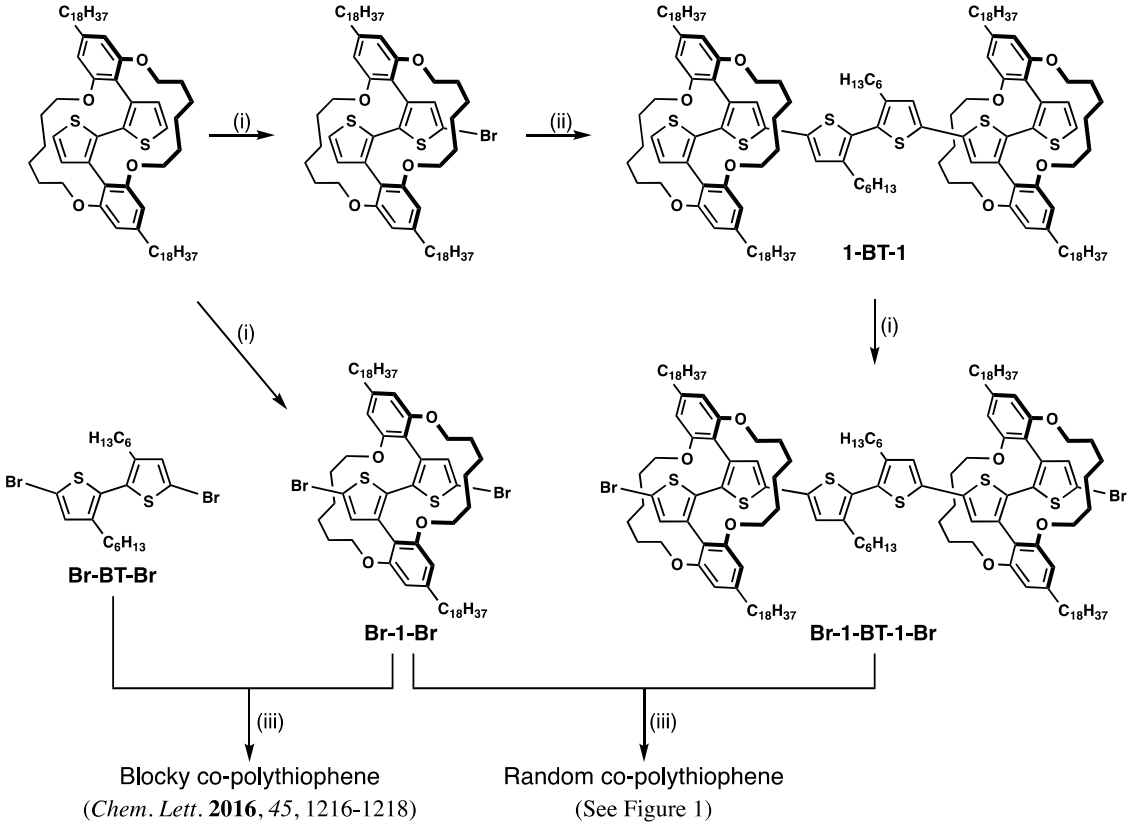

[a](i) NBS, THF, and RT; (ii) ^{i}PrMgCl, 5,5′-Dibromo-3,3′-dihexyl-2,2′-bithiophene, Pd(dppf)Cl2, THF, 80 °C; and (iii) Ni(COD)2, COD, bipy, Toluene/DMF, 90 °C.

molecular backbone,[13] coupled with other vibrational displacements. Different works describe how the most intense Raman bands (Я bands) are affected by the effective conjugation length of the polymer chains and how intramolecular and also intermolecular interactions can be investigated by analyzing the frequency and intensity pattern in Raman spectra.[14−17] An increase in π-conjugation often provokes a shift to a lower-frequency ν(Я) of the Я bands, and vice versa, a shift to a higher frequency is commonly related to systems where π-electrons are more confined.[13] In the case of a polyconjugated chain based on aromatic or heteroaromatic units, the extent of frequency dispersion of ν(Я) with chain length is strongly dependent on the aromaticity of constituent monomers.[18] In particular, oligothiophenes, phenylenes, and phenylene−vinylenes exhibit almost no frequency dispersion with the increase of the oligomer length,[18,19] while furan and pyrrole oligomers show a consistent degree of frequency dispersion.[19−21] To give a proper interpretation of the behavior of Raman spectra and to determine the relationship between the conjugation length and the structural, conformational, and morphological characteristics, calculations based on density functional theory (DFT) are often used, and it has been demonstrated to be very useful for the establishment of structure−property relationships.[17,19,20,22−24]

Recently, Sugiyasu et al.[25−30] have succeeded in the synthesis of insulated bithiophene-based oligomers and polymers with a polyrotaxane-like 3D architecture. The isolation of the polythiophene chain by rotaxination was designed to prevent electronic cross-communication between the adjacent polythiophene backbones and to facilitate the intrawire carrier transport pathways.[25,31] In fact, insulated molecular wires (IMWs) based on a fully encapsulated

https://doi.org/10.1021/acs.macromol.1c02458
Macromolecules 2022, 55, 3458−3468

polythiophene result in an excellent intrawire hole mobility of 0.9 $cm^2 V^{-1} s^{-1}$[25] thanks to the isolation of the π-conjugated backbones and to the stabilization of a quasi-planar conformation of the polythiophene sequence. Also, a myriad of properties has been reported for thiophene-based IMWs, allowing their use as polymer light-emitting diodes[28] or organic lasers,[32] among other interesting optoelectronic applications. Nevertheless, up to date, a detailed Raman characterization of polythiophene-based IMWs is still missing. In contrast, the investigation of the Raman properties of unsheathed polythiophenes, such as poly(3-hexylthiophene) P3HT,[22,33,34] where both intra- and intermolecular interactions would produce structural perturbation, has been widely investigated. Therefore, thiophene-based IMWs where $\pi-\pi$ interactions between adjacent conjugated chains are neglected constitute ideal test-beds to evaluate the changes in the molecular structure (*i.e.*, intrachain conformation and π-electron delocalization) within the conjugated polymer backbones.

In this context, we here investigate two series of polythiophene-based IMWs (see Figure 1) using a combined experimental and theoretical Raman study: (i) a fully insulated polymer and its corresponding oligomers (**IPT(0)** and **nIOT**, respectively; see Figure 1A,B) to qualitatively explore trends in π-conjugation with increasing the chain length. (ii) A new series of copolymers containing a controlled amount of twisted bithiophene units and planar insulated thiophene units (**IPT(N)** in Figure 1B, with a determined percentage (*N*%) of head-to-head defects) to investigate how the defect ratio impacts on the molecular structure and delocalization. To the best of our knowledge, this is the first time that an exhaustive Raman analysis of polythiophene-based IMWs is conducted.

MATERIALS AND METHODS

Synthesis of Partially Insulated Copolymers IPT(N). The head-to-head defect was randomly installed along the insulated polythiophenes, **IPT(N)**, the percentage of which (*N*%) is defined as the number of head-to-head linkages of the 3,3′-dihexyl-2,2′-bithiophene unit divided by the number of all of the $\alpha-\alpha$ linkages along the polythiophene chain (see details in the caption of Figure 1B). We have previously reported that copolymerization of **Br-1-Br** and 5,5′-dibromo-3,3′-dihexyl-2,2′-bithiophene (**Br-BT-Br**) yielded blocky copolymers because of the significant difference in the reactivity between these monomers.[27] Thus, we made a detour through synthesizing a sexithiophene consisting of **1** and bithiophene (Scheme 1). A mixture of **Br-1-Br** and **Br-1-BT-1-Br** at given molar ratios in toluene and DMF in the presence of bis(1,5-cyclooctadiene)-nickel(0), 2,2′-bipyridyl, and 1,5-cyclooctadiene was stirred at 90 °C for 3 days. After cooling to room temperature, 5 M aqueous hydrochloric acid was added to quench the reaction, the mixture was diluted with $CHCl_3$ and washed with the EDTA solution, $NaHCO_3$ solution, and then extracted with $CHCl_3$ three times. The combined organic layer was washed with brine and dried over $MgSO_4$. After the solvent was evaporated, the product was purified by reprecipitation and centrifugation (chloroform/acetone, 1 hour, 6000 rpm). We obtained **IPT(0)**, **IPT(0.96)**, **IPT(2.27)**, **IPT(4.17)**, **IPT(7.14)**, **IPT(9.38)**, **IPT(12.50)**, and **IPT(16.67)** from mixtures of **Br-1-Br** and **Br-1-BT-1-Br** in the ratios of 100:0, 98:2, 95:5, 90:10; 80:20, 70:30, 50:50, and 0:100, respectively.

Experimental Raman Measurements. Experimental Raman spectra were performed on the bulky solid-state sample at room temperature and atmospheric pressure conditions using three different excitation wavelengths. A Renishaw inVia Raman microscope (50× objective) was used to collect Raman spectra at 488 and 514 nm excitation wavelengths. Raman spectra were recorded with a laser power at, respectively, 0.03 and 0.012 mW, an acquisition time of 10 s, and a spectral resolution of 1 cm^{-1}. FT-Raman spectra (1064 nm excitation wavelength) were recorded with a RAM II Bruker VERTEX device with a spectral resolution of 4 cm^{-1} and by keeping the laser power below 10 mW. The intensities of the main components were evaluated by integrating the band inside a fixed bandwidth (FWHM of 20 cm^{-1}), while their frequencies were estimated as the center of a Lorentzian shape function, after a proper nonlinear fit.

Computational Methods. DFT calculations were performed using the Gaussian 09 software package.[35] Both the geometry optimization and prediction of Raman spectra have been carried out using the 6-31G(d,p) basis set[36−38] together with different DFT exchange−correlation functionals.

Three different hybrid functionals with different amounts of Hartree−Fock (HF) exchange were used: B3LYP[39,40] (20% HF exchange), the "half-and-half" hybrid functional BHLYP[41] (50% HF exchange, also referred to as BHandHLYP), and the PBE0[42] functional (25% HF exchange). The B3LYP functional has been shown to accurately reproduce the experimentally measured frequency of the Я mode in conjugated oligomers; however, it fails to predict the experimentally observed dispersion of the mode with oligomer length due to an overestimation of the π-delocalization. On the other hand, BHLYP has been found to predict very well the length-dependent trends in frequency dispersion observed for several conjugated materials.[19,20] Finally, PBE0 has been proved to be well suited for simulating the spectroscopic properties of carbon nanostructures.[43,44]

The vibrational analyses confirmed the convergence to stable molecular geometries inasmuch for all optimized structures no normal modes with imaginary frequencies have been predicted. For each functional and basis set, suitable frequency scaling factors were used to compare the computed vibrational spectra with the experimental one:[45] these factors are 0.965 for B3LYP, 0.931 for BHLYP, and 0.955 for PBE0.

In the framework of periodic boundary conditions (PBCs), DFT, full geometry optimization, and vibrational spectra calculations of the single infinite one-dimensional chain (1D) have been carried out, employing the CRYSTAL14 code with BHLYP functional and the 6-31G(d,p) basis set, considering both the fully insulated polymer (**IPT(0)**) and the partially unsheathed copolymer (**IPT(16.67)**) (see Figure 1B). In both the geometry optimization and Raman spectra calculations, we used shrinking factors (SHRINK parameter) of 20 (corresponding to 11 points in the Brillouin zone), TOLINTEG values of 8 8 8 9 30, an FMIXING of 30, and a tolerance on the change of total energies (TOLDEE parameter) of 8 (10^{-8} hartree) for geometry optimization and 10 for Raman calculations. The Raman spectra were simulated through the calculation of the static Raman tensors, i.e., in the limit of exciting wavelength $\lambda \rightarrow \infty$. This choice guaranteed an accurate description of the intensity pattern of the FT-Raman spectra (λ = 1064 nm) obtained experimentally for these systems.

RESULTS

In the first part of the present study, we characterize the Raman and conformational properties of a fully insulated polymer and their corresponding oligomers (**IPT(0)** and **nIOT**, respectively, in Figure 1A). The monomer consists of bithiophene with alkylene straps that doubly crossover the two resorcinol units.[25] Their UV/vis/NIR absorption and fluorescence measurements were previously reported by Sugiyasu et al.,[25] suggesting an extended π-electron delocalization in the backbone planarized by the alkylene straps. Furthermore, the backbone protection was found to dramatically reduce static (or ultrafast) fluorescence quenching[46] resulting in efficient amplified spontaneous emission.[32] In the second part, a new series of copolymers with a different degree (*N*% in **IPT(N)**; see Figure 1B) of the head-to-head defect (3,3′-dihexyl-2,2′-bithiophene unit) randomly installed along the 3D rotaxane-like structure are studied to evaluate the trend in π-

https://doi.org/10.1021/acs.macromol.1c02458
Macromolecules 2022, 55, 3458−3468

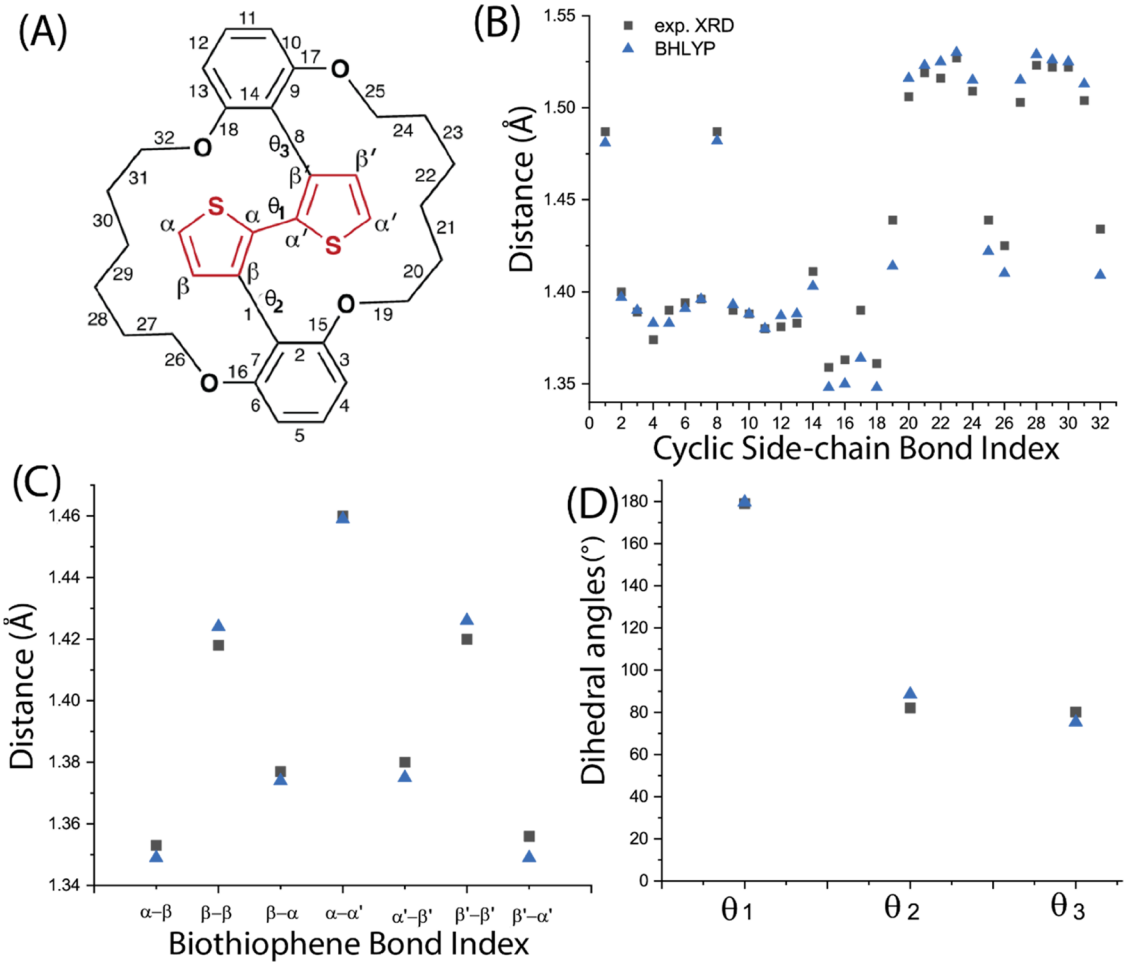

Figure 2. (A) Chemical structure of **1IOT** displaying the bond's labels used for the evaluation of bond lengths and dihedral angles. Graphical representation of the comparison between the DFT-calculated bond lengths along the cyclic side chain (B) and bithiophene backbone (C) and dihedral angles (D) using BHLYP functionals (blue marks) with those experimentally observed by X-ray (black marks). The legend in panel (B) applies to panels (C) and (D).

conjugational properties by increasing the defect ratio along the polythiophene backbone.

Fully Insulated nIOT Oligomers and IPT(0) Polymer. *DFT-Calculated Geometries.* Figure 2 compares the X-ray experimental and DFT-calculated bond lengths and inter-ring dihedral angles of **1IOT** monomer. Note that three functionals with different HF exchanges were tested (B3LYP, BHLYP, and PBE0), with BHLYP providing better agreement with the experiment (see Figure S1). The conjugated CC bond sequence inside the bithiophene units (see Figure 2C) shows that the conjugation path is characterized by the CC bond length alternation, with the longest CC bonds corresponding to the inter-ring one. Interestingly, the computed bond length alternation (BLA) parameter within the oligothiophene backbone for oligomers of an increasing size slightly changes with the oligomer length (*i.e.*, 0.070 Å for **1IOT** and 0.066 Å for **4IOT**; see Table 1), a behavior that is commonly encountered for polymers containing rings characterized by a high degree of aromaticity.[18,47]

On the other hand, two observations can be extracted from the trend shown by the computed dihedral angles around CC bonds linking thiophene rings in the oligomer series (see Table 1):

(i) The inter-ring dihedral angles θ between the self-threading bithiophene units is ∼180° regardless of the oligomer size (see Tables 1 and S2). This further proves the effectiveness of the constraint exerted by the encapsulating moiety in stabilizing a flat structure inside the sheathed bithiophene units.

(ii) The inter-ring dihedral angles θ between the self-threading dimers (θ_i, with i even value in Table 1) show moderate twisting distortions from planarity. Note that BHLYP predicts more distorted structures (*i.e.*, an average θ_i value of 165°; Table 1) than PBE0 and B3LYP functional do (*i.e.*, with average values θ_i of ∼175°; Table S2). Thus, we can argue that the π-electron conjugation along the molecular backbone results to be slightly lower when adopting the BHLYP functional. In fact, the BHLYP functional allows obtaining a remarkably better agreement with Raman experiments as it will be clear in the following.

Raman Characterization. Experimental FT-Raman spectra of the fully insulating polythiophene (**IPT(0)**) and its corresponding oligomers (**2IOT** to **5IOT**) are shown in Figure 3. The spectra are dominated by two main Raman bands observed at 1445 cm^{-1} (A band) and 1377 cm^{-1} (B band). The vibrational displacements associated with the A

https://doi.org/10.1021/acs.macromol.1c02458
Macromolecules 2022, 55, 3458−3468

Table 1. DFT-Calculated (BHLYP/6-31G) Bond Length Alternation (BLA) Values (a) and Dihedral Angle Values around CC Bonds Linking Thiophene Units (b) for 1IOT−4IOT Oligomers**[a]

(A)

	1IOT	2IOT	3IOT	4IOT
BLA (Å)	0.070	0.068	0.066	0.066

(B)

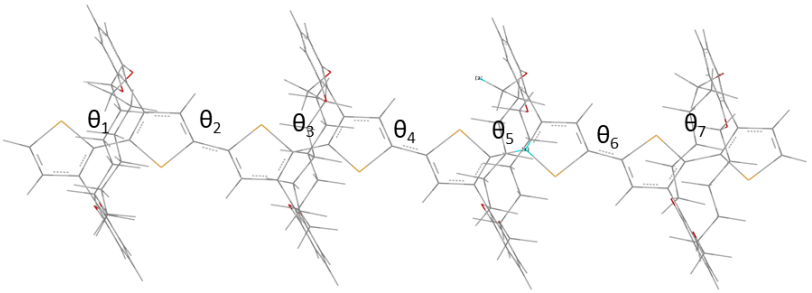

	Dihedral Angles (°)						
Compound	**θ_1**	**θ_2**	**θ_3**	**θ_4**	**θ_5**	**θ_6**	**θ_7**
1IOT	180						
2IOT	180	166	179				
3IOT	180	166	180	165	180		
4IOT	180	165	180	166	180	165	180

[a]The sketch illustrates the dihedral angle labeling adopted. BLA is calculated as the average bond length difference between quasi-single and quasi-double CC bonds along the conjugated backbone (CC bonds belonging to thiophene molecules and inter-ring CC bonds). Please see Table S2 for the results obtained at the PBE0/6-31G** and CAM-B3LYP/6-31G** levels.

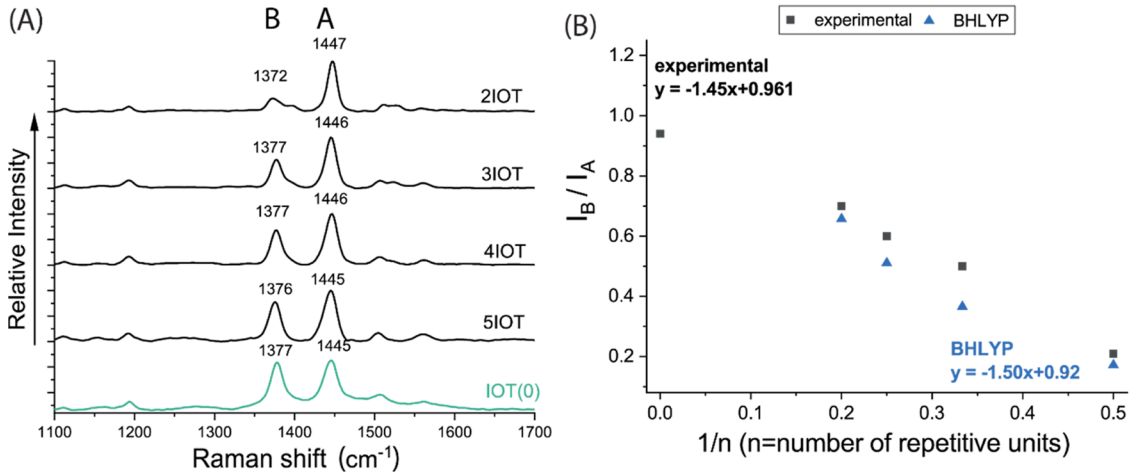

Figure 3. (A) Comparison of the FT-Raman spectra of nIOT oligomers (black lines) and the defect-free IPT(0) polymer (green line). Spectra are vertically shifted for clarity. (B) Comparison of the experimental and calculated I_B/I_A intensity ratios *vs* the reciprocal number of repetitive units. Equations in the graph describe the linear fitting on each data set.

band can be truly described as a collective Я mode since it involves—even if to a different extent—the whole set of CC stretching coordinates of the polythiophene backbone, whereas the vibrational mode responsible for the B band is more localized on the individual **IOT** dimers (see Table S3). Indeed, the detailed analysis of vibrational eigenvectors (Table S3)

https://doi.org/10.1021/acs.macromol.1c02458
Macromolecules 2022, 55, 3458−3468

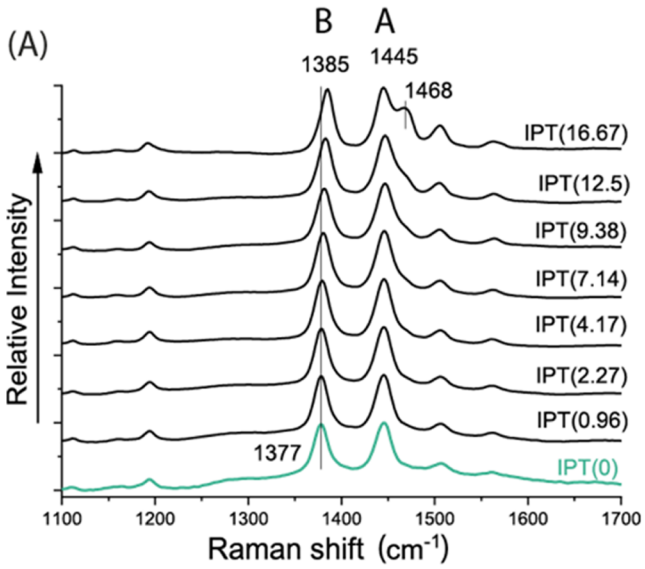

(B)

Polymer	I_B/I_A
IPT(0)	0.94
IPT(0.96)	0.93
IPT(2.27)	0.92
IPT(4.17)	0.91
IPT(7.14)	0.89
IPT(9.38)	0.83
IPT(12.4)	0.81
IPT(16.67)	0.80

Figure 4. (A) FT-Raman spectra comparison of the partially insulated (head-to-head defect) copolymers (black line) with different percentages of unsheathed units (*N*% in **IPT(N)**) and the fully insulated polymer, **IPT(0)** (green line). Spectra are vertically shifted for clarity. (B) Evolution of the I_B/I_A intensity ratio of the two main Raman components for defect copolymer.

computed for the polymer and the oligomers shows a rather complex vibrational structure, which is also discussed in depth in the SI.

The two main A and B Raman bands do not shift in frequency by increasing the length of the conjugated chain. This behavior is not surprising since it is also found for the Я band (at about 1445 cm^{-1}), which dominates the Raman spectrum of other variously substituted oligothiophenes, and has been discussed in several papers.[18,19,21,23] Interestingly, we observe that the ratio of the relative intensities of the two most intense Raman bands of the **nIOT** series ($I_{1377}/I_{1445} = I_B/I_A$) increases with chain length and does not saturate up to the polymer (see Figure S2).

For a better understanding of the experimental trend, we now make use of DFT calculations of the Raman spectra of the oligomer series (from **1IOT** to **4IOT**). The linear fit of I_B/I_A versus the inverse number of repetition units (1/n) (*i.e.*, compare the slopes of the straight lines reported inFigure 3B) highlights that the BHLYP functional provides a good description of the I_B/I_A ratio. However, B3LYP and PBE0 overestimate the intensity increase of the 1377 cm^{-1} component with respect to the 1445 cm^{-1}, giving an inversion in the I_B/I_A ratio in **4IOT** (see Figures S2 and S3). In addition, BHLYP predicts no frequency dispersion for the two main Raman bands in good accordance with the experimental observation, while B3LYP and PBE0 functionals reveal a progressive softening of the frequency of the A band at 1445 cm^{-1}, which shifts toward lower frequencies from **1IOT** to **4IOT** ($\Delta\nu$ = 11 and 15 cm^{-1}, respectively; see Figure S3). Thus, the BHLYP functional gives the best qualitative and quantitative descriptions of the evolution of the Raman spectra. Note that BHLYP was also found to provide very accurate trends of Я-mode dispersion with the increasing oligomer length in oligofurans and oligothiophenes.[19,20]

The above observations deserve a discussion, which can be done in the framework of ECC theory. ECC theory provides a common interpretative framework of the Raman spectra of several π-conjugated molecules and polymers, grounded on the observation that the oscillation of the bond length alternation (BLA),[48] *i.e.*, the vibration along the collective coordinate Я, determines a huge polarizability oscillation, $(\partial\alpha/\partial Я)$, which steeply increases in value with the conjugation length. This explains the very large Raman cross section of a few Raman transitions associated with normal modes showing a high Я contribution (Я modes).

The increase of the conjugation length can affect the Raman spectrum in different ways:

(i) Frequency softening of the Я modes, which is remarkably evident in the case of the polyenes and polyacetylene,[9,48] while it can be less evident (or even absent) in π-conjugated α-oligoheterocycles depending on the aromaticity of constituent rings.[16,18,20,21,23]

(ii) Modulation of the intensity pattern, resulting in an "intensity transfer" between Я bands. These intensity changes often reflect the evolution of the vibrational eigenvectors, while increasing the conjugation length. For the polyene series, this phenomenon is very pronounced and is rationalized, considering the leading role of the polarizability change associated with the BLA oscillation $(\partial\alpha/\partial Я)$ in Raman cross sections. Indeed, in the case of polyenes, the lower-frequency Я mode, parallel to its frequency softening, shows an increasingly large content of Я character—i.e., of collective BLA oscillation—while increasing the chain length.[9]

(iii) In the case of oligomers, peculiar effects related to the presence of end groups, whose localized vibrational displacements can couple in different ways with a collective Я-like vibration of the inner units, may affect the spectral pattern in various ways. In several cases, this results in the appearance of additional Raman features of the medium−weak intensity in the spectrum of short oligomers.[21]

The two phenomena (i) and (ii) are strongly entangled: this is probably the reason why, in the case under investigation, B3LYP and PBE0 functionals—that overestimate π-electron delocalization—not only predict the occurrence of the frequency dispersion but also overestimate the intensity transfer between Я modes.

https://doi.org/10.1021/acs.macromol.1c02458
Macromolecules 2022, 55, 3458−3468

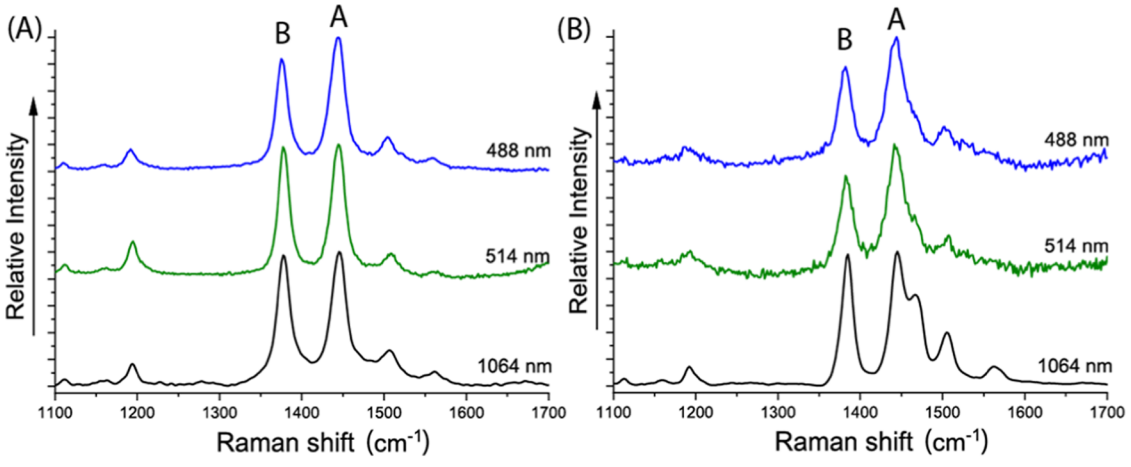

(C)

	Compound	488 nm	514 nm	1064 nm
I_B/I_A	**IPT(0)**	0.773	0.810	0.940
	IPT(0.96)	0.770	0.805	0.933
	IPT(4.17)	0.765	0.795	0.912
	IPT(16.67)	0.644	0.790	0.804

Figure 5. Experimental Raman spectra of **IPT(0)** (A) and **IPT(16.67)** polymers (B) recorded at different excitation wavelengths (488, 514, and 785 nm), and evolution of the I_B/I_A intensity ratio for **IPT(0)**, **IPT(0.96)**, **IPT(4.17)**, and **IPT(16.67)** polymers at different excitation wavelengths (C).

In the **nIOT** series, we experimentally observe for the first time the occurrence of the intensity transfer between the two main Raman bands, without any significant frequency softening. Both (ii) and (iii) phenomena might determine the observed behavior.

In this regard, it is interesting to note that only the functional BHLYP takes the experimental intensity behavior fully into account, showing that the observed trend can be faithfully reproduced if the description of the π-delocalization is perfectly balanced. For this peculiar family of molecules, BHLYP seems to provide the best compromise.

For this reason, we focused on BHLYP results for a detailed analysis of vibrational eigenvectors and local Raman intensity parameters, aiming at understanding the origin of the observed intensity trend. The discussion concerns DFT calculations carried out for the polymer and **nIOT** oligomers (n = 2−4) and is illustrated in detail in the SI (Table S3). The relevant conclusion of this analysis is that the increase of the Raman intensity with the conjugation length is steeper for the B band than for the A band because modes associated with the B features show a large contribution of stretchings of the quasi-single C−C bonds. Indeed, $\partial\alpha/\partial R_i$ associated with the stretching of the single C−C bonds are more sensitive to the conjugation length than polarizability derivatives with respect to C═C bond stretchings.

Partially Insulated Copolymers IPT(N) with Head-to-Head Defects along the Chain. *Experimental Raman Characterization.* The FT-Raman spectra of copolymers with an increased percentage (N%) of head-to-head defects (unsheathed bithiophene units) randomly placed along the chain are displayed in Figure 4. The Raman data reveal a similar trend to that observed in the fully insulated **nIOT** oligomers with the following analogies: (i) the A and B modes are the most intense Raman bands of the spectra, (ii) no frequency dispersion of the collective Я mode at 1445 cm^{-1} is observed upon increasing the number of defects or unsheathed units in the copolymer structure, and (iii) an intensity transfer of the two main Raman bands is found as a function of the defect rate. In line with this last point, a decrease of the I_B/I_A intensity ratio is recorded when increasing the defect ratio (*i.e.*, when increasing the number of nonencapsulated or unsheathed units *vs* insulated units). This evidence suggests that the head-to-head defects determine a conformational distortion of the polythiophene backbone and a consequent reduction of π-electron delocalization, as will be discussed below by DFT calculations.

The experimental Raman spectra reported in Figure 4 show additional interesting features, namely, (a) a new Raman component at a higher frequency (shoulder at 1468 cm^{-1}) clearly appeared for the copolymers with the highest defect rate: this is a marker band of the defect, as shown below with the help of the DFT calculations; and (b) the lower-frequency mode at 1377 cm^{-1} exhibits a red shift up to 1385 cm^{-1} (+7 cm^{-1}) when going from the fully insulated polymer (N% = 0, equivalent to **IPT(0)** polymer) to that with the maximum percentage of defects (N% = 16.67, equivalent to **IPT(16.67)** polymer).

The Raman spectra at different excitation wavelengths (see Figure 5) for fully insulated polymers and selected partially insulated copolymers (N% = 0.96, 4.17, and 16.67) confirm the same trend on different samples for both frequency and intensity ratio when increasing the percentage of head-to-head defects (N%), thus, ruling out the dependence of the Raman spectra on the excitation line adopted or the occurrence of relevant resonance/preresonance effect. However, a closer look at the intensity pattern (Figure 5C) shows an interesting

https://doi.org/10.1021/acs.macromol.1c02458
Macromolecules 2022, 55, 3458−3468

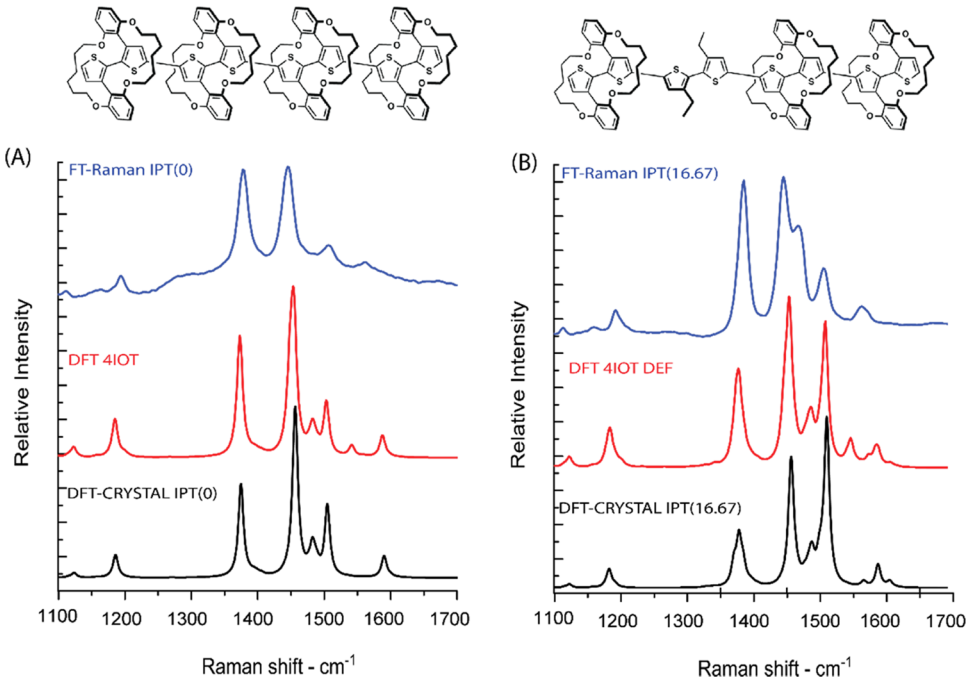

Figure 6. Experimental (blue lines) and DFT-calculated Raman spectra (model oligomers, red lines; polymers, black lines) of the fully insulated **IPT(0)** polymer (a) and partially insulated **IPT(16.67)** polymer (b). Chemical structures of the unit cell used for polymer calculations are reported on top. The model oligomers used for the calculations of the fully and partially insulated polymers correspond to **4IOT** and its homologue system containing one defect denoted as **4IOT-DEF**.

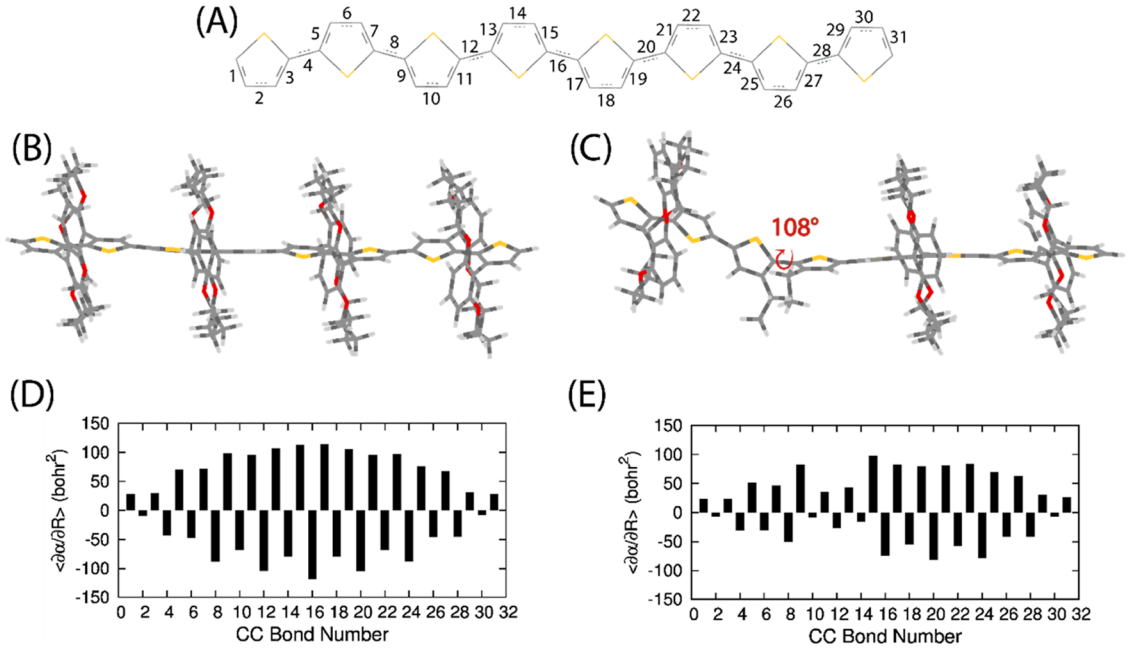

Figure 7. Comparison of computed Raman parameters relative to the CC bonds along the backbone chain for fully and partially insulated polymers within the oligomer approach (4 units). (A) The numbering of the CC bonds in the conjugated pathway. (B, C) Lateral views of the optimized (at the BHLYP/6-31G** level) structure of **4IOT** and **4IOT-DEF** as models for the fully insulated polymer and head-to-head copolymer, respectively. In panel (C), the dihedral angle value between the unsheathed bithiophene unit is shown in red (108°). (D, E) Trace of the CC stretching polarizability tensor $\partial\alpha/\partial R_i$ of **4IOT** and **4IOT-DEF**.

phenomenon: for each sample (same *N*%), the intensity ratio I_B/I_A slightly increased by exciting with longer excitation wavelengths (lower excitation energy; *i.e.*, 1064 nm). This evidence can be related to the moderate polydispersity of these polymers (PDI 2−2.5) for which the presence of chains with different weights/lengths can be assumed. Moreover, also the presence of the chemical defects could determine a distribution of different conjugation lengths in each chain and in the whole sample, especially when it is accompanied by conformational distortion.

Thus, the observed increase of I_B/I_A with longer excitation wavelengths is proof that this parameter is an index of the π-

https://doi.org/10.1021/acs.macromol.1c02458
Macromolecules 2022, 55, 3458−3468

delocalization for polythiophene-insulated molecular wires. All of these experimental evidence on the partially insulated copolymers with different defect rates, in the light of the findings for oligomers' results and the wide literature on conjugated polymers,[13,20,49] suggested a decrease of the π-electron delocalization of the backbone when increasing the number of unsheathed units.

DFT Calculations. The insulated polymers were simulated within the oligomer approach using a model system of four oligomer units (the fully and partially insulated model oligomers are denoted as **4IOT** and **4IOT-DEF**, respectively; see Figure 6). In addition, periodic boundary conditions were applied on the chain axis direction with the CRYSTAL code to model an infinite one-dimensional polymer chain, mimicking a regular copolymer with a unit cell containing three encapsulated units and one unsheathed bithiophene unit.

Figure 6 displays the simulated Raman spectra of the **IPT(16.67)** using both models (oligomer and polymer). Despite the simplified models adopted, which cannot describe the variety of intramolecular environments experienced by chains in the real **IPT(16.67)** samples, namely, the presence of a variety of chain conformations, in conjunction with a random distribution of defects, the most relevant experimental features are qualitatively reproduced. The calculations nicely describe:

(i) The splitting of the Я mode, which gives rise to a new, strong Raman band detectable as a shoulder on the higher-frequency side of the main band of **IPT(16.67)** and absent in **IPT(0)**. The predicted frequency (~1500 cm^{-1}) of this high-frequency band is overestimated by the calculations, probably because of the oversimplification of our model, but it reasonably explains the nature of the observed shoulder at 1468 cm^{-1}. According to the vibrational eigenvectors computed for the partially insulated **4IOT-DEF** model system and for its analogue 1D-polymer (see sketches reported in Figure S4 and Table S4), this band is attributed to the occurrence of a Я mode mainly localized on the unsheathed head-to-head bithiophene units.

(ii) The decrease of the I_A/I_B ratio when the percentage of the defects (*i.e.*, *N*%) increases. This can be ascribed to the fact that the insertion of bithiophene units without the cyclic side-chain protection leads to more distorted structures; indeed, a torsional angle between the two nonprotected thiophene units of about 108° is predicted for **4IOT-DEF**, resulting in a reduction of π-delocalization (see Figure 7).

Finally, interesting information on π-delocalization of these insulated polythiophenes can be gained by looking at the computed Raman parameters within the oligomer approach (Figure 7). The values of the individual $\partial\alpha/\partial R_i$ parameters presented in Figure 7 allow rationalizing changes in experimental Raman Intensities. In panels (D) and (E), the $\partial\alpha/\partial R_i$ values are compared for **4IOT** and **4IOT-DEF** oligomers. The pattern of $\partial\alpha/\partial R_i$ in the proximity of the defect unit (Figure 7E) shows absolute values significantly lower than those to the end (rotaxinated) units and those calculated for the fully insulated or defect-free system (Figure 7D); moreover, $\partial\alpha/\partial R_{C\text{-}C}$ parameters involving CC single bond stretchings (bonds 10, 12, 14; see the figure) localized on the unsheathed bithiophene unit show a remarkable decrease in their absolute value. This phenomenon is responsible for a more marked intensity decrease of the B band with respect to the A-feature upon increasing the defect content, thus, explaining the observed decrease of the I_B/I_A ratio. The subtle mechanism, which justifies the decrease of I_A/I_B, parallels what has already been rationalized in the case of **nIOT** oligomers (see detailed discussion in the SI) and further supports the use of this parameter for a diagnosis of the degree of π-electron delocalization.

CONCLUSIONS

In this work, we carried out a detailed Raman characterization of fully and partially insulated polythiophene-based molecular wires. Experimental evidence and DFT calculations reveal the presence of two Я Raman modes (at 1377 and 1445 cm^{-1} denoted as B and A, respectively), which exhibit an intensity transfer while varying the extent of π-conjugation of the system. In fact, when comparing the fully insulated **IPT(0)** polymer with their corresponding **nIOT(n)** oligomers, the observed I_A/I_B intensity ratio is found to increase. The same trend has been properly predicted by DFT calculations with the BHLYP functional, providing better agreement with experiments. On the other hand, when increasing the defect ratio in the new series of partially insulated copolymers **IPT(N)**, a decrease of the I_A/I_B intensity ratio is observed together with the appearance of a new Raman band at ~1468 cm^{-1}, which is ascribed to a Я mode mainly localized on the unsheathed bithiophene units. This is ascribed to the fact that the insertion of nonencapsulated bithiophene units leads to more distorted structures, which, in turn, results in a reduction of π-delocalization.

In summary, this study demonstrates that the intensity pattern between the two main CC stretching Raman bands (I_A/I_B) can be taken as a marker of the π-delocalization for polythiophene-insulated molecular wires, retrieving very important information about the conjugation length and conformational disorder of these systems. This structural information can be very useful to shed light on the carrier transport pathways and other important electronic processes of organic conjugated polymers in which the intrachain conformation and π-delocalization play an active role.

ASSOCIATED CONTENT

Supporting Information

The Supporting Information is available free of charge at https://pubs.acs.org/doi/10.1021/acs.macromol.1c02458.

Synthetic procedures; DFT-calculated dihedral angles and bond lengths and Raman spectra for **IPT(0)** polymer and **nIOT** oligomers when using BHLYP, PBE0, and B3LYP functionals; DFT-calculated vibrational eigenvectors (at the BHLYP level) for **nIOT** oligomers, **IPT(0)** polymer, and for a model polymer with a repeating unit consisting of two encapsulated bithiophene units and one nonencapsulated bithiophene unit; DFT-calculated values of the Raman parameters of two trans-polyene models with different lengths; and a detailed discussion about the modulation of the relative Raman intensities for nIOT oligomers (PDF)

AUTHOR INFORMATION

Corresponding Authors

Chiara Castiglioni − *Dipartimento di Chimica, Materiali e Ingegneria Chimica, Politecnico di Milano, 20133 Milano,*

https://doi.org/10.1021/acs.macromol.1c02458
Macromolecules 2022, 55, 3458−3468

Italy; orcid.org/0000-0002-6945-9157; Email: chiara.castiglioni@polimi.it

M. Carmen Ruiz Delgado − *Department of Physical Chemistry, University of Málaga, 229071 Málaga, Spain*; orcid.org/0000-0001-8180-7153; Email: carmenrd@uma.es

Authors

Sara Mosca − *Central Laser Facility, Research Complex at Harwell, STFC Rutherford Appleton Laboratory, UK Research and Innovation, OX11 0QX Didcot, U.K.*; orcid.org/0000-0001-9479-5614

Alberto Milani − *Dipartimento di Energia, Politecnico di Milano, 20133 Milano, Italy*; orcid.org/0000-0001-6026-5455

Víctor Hernández Jolín − *Department of Physical Chemistry, University of Málaga, 229071 Málaga, Spain*

Cristóbal Meseguer − *Department of Physical Chemistry, University of Málaga, 229071 Málaga, Spain*

Juan T. López Navarrete − *Department of Physical Chemistry, University of Málaga, 229071 Málaga, Spain*

Chunhui Zhao − *Molecular Design & Function Group, National Institute for Material Science, Tsukuba, Ibaraki 305-0047, Japan*

Kazunori Sugiyasu − *Molecular Design & Function Group, National Institute for Material Science, Tsukuba, Ibaraki 305-0047, Japan*; orcid.org/0000-0001-5699-2772

Complete contact information is available at: https://pubs.acs.org/10.1021/acs.macromol.1c02458

Notes

The authors declare no competing financial interest.

■ ACKNOWLEDGMENTS

This work at the University of Málaga was funded by the MICINN (PID2019-110305GB-I00) and Junta de Andalucía (UMA18-FEDERJA-080, P09FQM-4708, and P18-FR-4559) projects. The authors thankfully acknowledge the computer resources, technical expertise, and assistance provided by the SCBI (Supercomputing and Bioinformatics) Center of the University of Malaga. Funding for open access charge: Universidad de Málaga / CBUA.

■ REFERENCES

(1) Skotheim, T. A.; Reynolds, J. R. *Handbook of Conducting Polymers: Conjugated Polymers Processing and Applications*, 3rd ed.; CRC: Boca Raton, FLA, 2007; Vol. 2, p. 823.

(2) Skotheim, T. A.; Reynolds, J. R. *Conjugated Polymers: Theory, Synthesis, Properties, and Characterization*, CRC: Boca Raton, Fla, 2006; pp 15−22.

(3) Kaur, N.; Singh, M.; Pathak, D.; Wagner, T.; Nunzi, J. M. Organic Materials for Photovoltaic Applications: Review and Mechanism. *Synth. Met.* **2014**, *190*, 20−26.

(4) Groves, C. Organic Light-Emitting Diodes: Bright Design. *Nat. Mater.* **2013**, *12*, 597−598.

(5) Åslund, A.; Nilsson, K. P. R.; Konradsson, P. Fluorescent Oligo and Poly-Thiophenes and Their Utilization for Recording Biological Events of Diverse Origin−When Organic Chemistry Meets Biology. *J. Chem. Biol.* **2009**, *2*, 161−175.

(6) Wang, C.; Dong, H.; Hu, W.; Liu, Y.; Zhu, D. Semiconducting π-Conjugated Systems in Field-Effect Transistors: A Material Odyssey of Organic Electronics. *Chem. Rev.* **2012**, *112*, 2208−2267.

(7) Le, T.-H.; Kim, Y.; Yoon, H. Electrical and Electrochemical Properties of Conducting Polymers. *Polymers* **2017**, *9*, 150.

(8) Jackson, N. E.; Kohlstedt, K. L.; Savoie, B. M.; Olvera De La Cruz, M.; Schatz, G. C.; Chen, L. X.; Ratner, M. A. Conformational Order in Aggregates of Conjugated Polymers. *J. Am. Chem. Soc.* **2015**, *137*, 6254−6262.

(9) Castiglioni, C.; Tommasini, M.; Zerbi, G. Raman Spectroscopy of Polyconjugated Molecules and Materials: Confinement Effect in One and Two Dimensions. *Philos. Trans. R. Soc., A* **2004**, *362*, 2425−2459.

(10) Nguyen, T.-Q.; Martini, I. B.; Liu, J.; Schwartz, B. J. Controlling Interchain Interactions in Conjugated Polymers: The Effects of Chain Morphology on Exciton−Exciton Annihilation and Aggregation in MEH−PPV Films. *J. Phys. Chem. B* **2000**, *104*, 237−255.

(11) Castiglioni, C.; Lopez Navarrete, J. T.; Zerbi, G.; Gussoni, M. A Simple Interpretation of the Vibrational Spectra of Undoped, Doped and Photoexcited Polyacetylene: Amplitude Mode Theory in the GF Formalism. *Solid State Commun.* **1988**, *65*, 625−630.

(12) Lopez-Navarrete, J. T.; Tian, B.; Zerbi, G. Relation between Effective Conjugation, Vibrational Force Constants and Electronic Properties in Polyconjugated Materials. *Solid State Commun.* **1990**, *74*, 199−202.

(13) Burrezo, P. M.; Zafra, J. L.; López Navarrete, J. T.; Casado, J. Quinoidal/Aromatic Transformations in π-Conjugated Oligomers: Vibrational Raman Studies on the Limits of Rupture for π-Bonds. *Angew. Chem. Int. Ed.* **2017**, *56*, 2250−2259.

(14) Schaffer, H. E.; Chance, R. R.; Silbey, R. J.; Knoll, K.; Schrock, R. R. Conjugation Length Dependence of Raman Scattering in a Series of Linear Polyenes: Implications for Polyacetylene. *J. Chem. Phys.* **1991**, *94*, 4161.

(15) Gussoni, M.; Castiglioni, C.; Zerbi, G. Vibrational Spectroscopy of Conducting Polymers. *Spectrosc. Adv. Mater.* **1991**, *19*, 355−396.

(16) Ferrón, C. C.; Sheynin, Y.; Li, M.; Patra, A.; Bendikov, M.; López Navarrete, J. T.; Hernández, V.; Ruiz Delgado, M. C. Raman Spectroscopic Characterization of Polyselenophenes and Poly(3,4-Ethylenenedioxyselenophene)S. *Isr. J. Chem.* **2014**, *54*, 759−766.

(17) Mosca, S.; Milani, A.; Peña-Álvarez, M.; Yamaguchi, S.; Hernández, V.; Ruiz Delgado, M. C.; Castiglioni, C. Mechanochromic Luminescent Tetrathiazolylthiophenes: Evaluating the Role of Intermolecular Interactions through Pressure and Temperature-Dependent Raman Spectroscopy. *J. Phys. Chem. C* **2018**, *122*, 17537−17543.

(18) Hernandez, V.; Castiglioni, C.; Del Zoppo, M.; Zerbi, G. Confinement Potential and π-Electron Delocalization in Polyconjugated Organic Materials. *Phys. Rev. B* **1994**, *50*, 9815−9823.

(19) Donohoo-Vallett, P. J.; Bragg, A. E. π-Delocalization and the Vibrational Spectroscopy of Conjugated Materials: Computational Insights on Raman Frequency Dispersion in Thiophene, Furan, and Pyrrole Oligomers. *J. Phys. Chem. B* **2015**, *119*, 3583−3594.

(20) Ferrón, C. C.; Delgado, M. C. R.; Gidron, O.; Sharma, S.; Sheberla, D.; Sheynin, Y.; Bendikov, M.; Navarrete, J. T. L.; Hernández, V. α-Oligofurans Show a Sizeable Extent of π-Conjugation as Probed by Raman Spectroscopy. *Chem. Commun.* **2012**, *48*, No. 6732.

(21) Agosti, E.; Rivola, M.; Hernandez, V.; Zoppo, M.; Del; Zerbi, G. Electronic and Dynamical Effects from the Unusual Features of the Raman Spectra of Oligo and Polythiophenes. *Synth. Met.* **1999**, *100*, 101−112.

(22) Tsoi, W. C.; James, D. T.; Kim, J. S. J. S.; Nicholson, P. G.; Murphy, C. E.; Bradley, D. D. C.; Nelson, J.; Kim, J. S. J. S. The Nature of In-Plane Skeleton Raman Modes of P3HT and Their Correlation to the Degree of Molecular Order in P3HT:PCBM Blend Thin Films. *J. Am. Chem. Soc.* **2011**, *133*, 9834−9843.

(23) Milani, A.; Brambilla, L.; Del Zoppo, M.; Zerbi, G. Raman Dispersion and Intermolecular Interactions in Unsubstituted Thiophene Oligomers. *J. Phys. Chem. B* **2007**, *111*, 1271−1276.

(24) Sousa, S. F.; Fernandes, P. A.; Ramos, M. J. General Performance of Density Functionals. *J. Phys. Chem. A* **2007**, *111*, 10439−10452.

(25) Sugiyasu, K.; Honsho, Y.; Harrison, R. M.; Sato, A.; Yasuda, T.; Seki, S.; Takeuchi, M. A Self-Threading Polythiophene: Defect-Free

Insulated Molecular Wires Endowed with Long Effective Conjugation Length. *J. Am. Chem. Soc.* **2010**, *132*, 14754−14756.
(26) Ouchi, Y.; Sugiyasu, K.; Ogi, S.; Sato, A.; Takeuchi, M. Synthesis of Self-Threading Bithiophenes and Their Structure-Property Relationships Regarding Cyclic Side-Chains with Atomic Precision. *Chem. - An Asian J.* **2012**, *7*, 75−84.
(27) Zhao, C.; Takeuchi, M.; Sugiyasu, K. Synthesis of Unsheathed Insulated Molecular Wires. *Chem. Lett.* **2016**, *45*, 1216−1218.
(28) Méhes, G.; Pan, C.; Bencheikh, F.; Zhao, L.; Sugiyasu, K.; Takeuchi, M.; Ribierre, J. C.; Adachi, C. Enhanced Electroluminescence from a Thiophene-Based Insulated Molecular Wire. *ACS Macro Lett.* **2016**, *5*, 781−785.
(29) Shomura, R.; Sugiyasu, K.; Yasuda, T.; Sato, A.; Takeuchi, M. Electrochemical Generation and Spectroscopic Characterization of Charge Carriers within Isolated Planar Polythiophene. *Macromolecules* **2012**, *45*, 3759−3771.
(30) Pan, C.; Sugiyasu, K.; Wakayama, Y.; Sato, A.; Takeuchi, M. Thermoplastic Fluorescent Conjugated Polymers: Benefits of Preventing π-π Stacking. *Angew. Chem.* **2013**, *125*, 10975−10979.
(31) Cornil, B. J.; Beljonne, D.; Calbert, J.; Brødas, J.; Cornil, J.; Beljonne, D.; Calbert, J.; Brédas, J.-L. Interchain Interactions in Organic P-Conjugated Materials: Impact on Electronic Structure, Optical Response, and Charge Transport. *Adv. Mater.* **2001**, *13*, 1053−1067.
(32) Sun, C.; Mróz, M. M.; Castro Smirnov, J. R.; Lüer, L.; Hermida-Merino, D.; Zhao, C.; Takeuchi, M.; Sugiyasu, K.; Cabanillas-González, J. Amplified Spontaneous Emission in Insulated Polythiophenes. *J. Mater. Chem. C* **2018**, *6*, 6591−6596.
(33) Gao, Y.; Grey, J. K. Resonance Chemical Imaging of Polythiophene/Fullerene Photovoltaic Thin Films: Mapping Morphology-Dependent Aggregated and Unaggregated C═C Species. *J. Am. Chem. Soc.* **2009**, *131*, 9654−9662.
(34) Wu, L.; Casado, S.; Romero, B.; Otón, J. M.; Morgado, J.; Müller, C.; Xia, R.; Cabanillas-Gonzalez, J. Ground State Host−Guest Interactions upon Effective Dispersion of Regioregular Poly(3-Hexylthiophene) in Poly(9,9-Dioctylfluorene-Alt-Benzothiadiazole). *Macromolecules* **2015**, *48*, 8765−8772.
(35) Frisch, M. J.; Trucks, G. W.; Schlegel, H. B.; Scuseria, G. E.; Robb, Ma.; Cheeseman, J. R.; Scalmani, G.; Barone, V.; Petersson, Ga.; Nakatsuji, H.; Li, X.; Caricato, M.; Marenich, aV.; Bloino, J.; Janesko, B. G.; Gomperts, R.; Mennucci, B.; Hratchian, H. P.; Ortiz, J. V.; Izmaylov, aF.; Sonnenberg, J. L.; Williams; Ding, F.; Lipparini, F.; Egidi, F.; Goings, J.; Peng, B.; Petrone, A.; Henderson, T.; Ranasinghe, D.; Zakrzewski, V. G.; Gao, J.; Rega, N.; Zheng, G.; Liang, W.; Hada, M.; Ehara, M.; Toyota, K.; Fukuda, R.; Hasegawa, J.; Ishida, M.; Nakajima, T.; Honda, Y.; Kitao, O.; Nakai, H.; Vreven, T.; Throssell, K.; Montgomery, Ja., Jr.; Peralta, J. E.; Ogliaro, F.; Bearpark, M. J.; Heyd, J. J.; Brothers, E. N.; Kudin, K. N.; Staroverov, V. N.; Keith, Ta.; Kobayashi, R.; Normand, J.; Raghavachari, K.; Rendell, aP.; Burant, J. C.; Iyengar, S. S.; Tomasi, J.; Cossi, M.; Millam, J. M.; Klene, M.; Adamo, C.; Cammi, R.; Ochterski, J. W.; Martin, R. L.; Morokuma, K.; Farkas, O.; Foresman, J. B.; Fox, D. J.. *Gaussiann 09*. Revision B.01. Gaussian, Inc., 2009.
(36) Hariharan, P. C.; Pople, J. A. The Influence of Polarization Functions on Molecular Orbital Hydrogenation Energies. *Theor. Chim. Acta* **1973**, *28*, 213−222.
(37) Hehre, W. J.; Ditchfield, K.; Pople, J. A. Self-Consistent Molecular Orbital Methods. XII. Further Extensions of Gaussian-Type Basis Sets for Use in Molecular Orbital Studies of Organic Molecules. *J. Chem. Phys.* **1972**, *56*, 2257.
(38) Francl, M. M.; Pietro, W. J.; Hehre, W. J.; Binkley, J. S.; Gordon, M. S.; DeFrees, D. J.; Pople, J. A. Self-Consistent Molecular Orbital Methods. XXIII. A Polarization-Type Basis Set for Second-Row Elements. *J. Chem. Phys.* **1982**, *77*, 3654.
(39) Lee, C.; Yang, W.; Parr, R. G. Development of the Colle-Salvetti Correlation-Energy Formula into a Functional of the Electron Density. *Phys. Rev. B* **1988**, *37*, 785−789.
(40) Becke, A. D. Density-functional Thermochemistry. III. The Role of Exact Exchange. *J. Chem. Phys.* **1993**, *98*, 5648−5652.
(41) Becke, A. D. A New Mixing of Hartree−Fock and Local Density-functional Theories. *J. Chem. Phys.* **1993**, *98*, 1372−1377.
(42) Adamo, C.; Barone, V. Toward Reliable Density Functional Methods without Adjustable Parameters: The PBE0 Model. *J. Chem. Phys.* **1999**, *110*, 6158−6170.
(43) Milani, A.; Tommasini, M.; Barbieri, V.; Lucotti, A.; Russo, V.; Cataldo, F.; Casari, C. S. Semiconductor-to-Metal Transition in Carbon-Atom Wires Driven by Sp2 Conjugated End Groups. *J. Phys. Chem. C* **2017**, *121*, 10562−10570.
(44) Serafini, P.; Milani, A.; Tommasini, M.; Castiglioni, C.; Casari, C. S. Raman and IR Spectra of Graphdiyne Nanoribbons. *Phys. Rev. Mater.* **2020**, *4*, No. 014001.
(45) Laury, M. L.; Carlson, M. J.; Wilson, A. K. Vibrational Frequency Scale Factors for Density Functional Theory and the Polarization Consistent Basis Sets. *J. Comput. Chem.* **2012**, *33*, 2380−2387.
(46) Sahoo, D.; Sugiyasu, K.; Tian, Y.; Takeuchi, M.; Scheblykin, I. G. Effect of Conjugated Backbone Protection on Intrinsic and Light-Induced Fluorescence Quenching in Polythiophenes. *Chem. Mater.* **2014**, *26*, 4867−4875.
(47) Fazzi, D.; Canesi, E. V.; Negri, F.; Bertarelli, C.; Castiglioni, C. Biradicaloid Character of Yhiophene-Based Heterophenoquinones: The Role of Electron-Phonon Coupling. *ChemPhysChem* **2010**, *11*, 3685−3695.
(48) Gussoni, M.; Castiglioni, C.; G, Z. Vibrational Spectroscopy of Polyconjugated Materials: Polyacetylene and Polyenes. In *Advances in Material Science Spectroscopy*, Clark, H.; E, R.; Hester, E., Eds.; Wiley: New York, 1991; pp 251−353.
(49) Castiglioni, C.; Delzoppo, M.; Zerbi, G. Vibrational Raman-Spectroscopy of Polyconjugated Organic Oligomers and Polymers. *J. Raman Spectrosc.* **1993**, *24*, 485−494.

https://doi.org/10.1021/acs.macromol.1c02458
Macromolecules 2022, 55, 3458−3468